Chapter 17
Evaluation of Camera-Denoising Techniques towards Force Reconstruction

Sean Collier, Jonathan Young, Hruday Shah, Nicholas Vlajic, and Tyler Dare

Abstract Due to an abundance of spatial points, camera-based surface vibrations promise reduced testing times, higher resolution in response measurements, and the data necessary to over-constrain historically poor inverse problems in structural dynamics. For example, initial studies and formulations of a camera-based, modal force reconstruction (MFR) technique show great success and utility, but is highly sensitive to measurement noise—something abundant in camera data. The improvement of camera data has become a devoted effort in recent years, theoretically providing the path necessary to facilitate the use of MFR on realistic data. Such methods proposed range from simple singular value decomposition to those enforcing physical constraints on the measured response using additional accelerometers. To that end, this paper explores a variety of these camera-denoising techniques, their efficacy, and their utility towards improving measured displacements of a simple, pinned plate and cantilevered beam for use in modal force reconstruction.

Keywords Vibration · Denoising · Camera-Based · Decomposition · Substructuring

Introduction

Here we discuss camera noise and its role as a major drawback of a purely vision-based analysis. Indeed, while the efficacy of camera-based surface vibration measurement has seen increasing interest and characterization, its utility is far more limited compared to a laser or accelerometer in terms of noise floor and frequency detection. This limitation is clear from much of the authors' work alone [1–3], but is evident across the literature simply by the amount of work dedicated to the refinement of a purely camera-based vibration-measurement technique [4–10]. The aim of this work is to compare the utility of such camera denoising techniques towards the eventual use within camera-based modal force reconstruction, which has been observed to be plausible but prone to over-fitting of higher order modes in the presence of typical measurement noise. While regularization with a reduced number of modes has shown some success, further improvement to the technique requires improvement to the measurement quality. Thankfully, much work has been done for the improvement of noisy high speed camera data.

The first approach mentioned here is one that follows naturally from one-dimensional signal processing. If one follows the standard neighborhood assumptions of optical flow—especially if the object is captured with high resolution—then a local averaging around the pixel of interest is easy to implement and rather effective [10–14]. For example, it was shown in [1] that a local average around a pixel of interest was able to reduce the noise floor well enough to resolve motions originally obscured. While this approach is highly effective at interrogating a single point, such averaging may not be ideal when high spatial resolution is needed (e.g., spatial derivatives), or in the case where the measurement is not spatially dense across the structure. Thus, maintaining the spatial benefit of the measurement while also improving signal-to-noise requires more capable and general techniques.

One such technique comes from the use of data reduction methods, and the tendency of noise to fall within higher-

Sean Collier · Jonathan Young · Nicholas Vlajic · Tyler Dare
The Pennsylvania State University, University Park, PA 16804
e-mail: smc604@psu.edu; juy218@psu.edu; nav5000@psu.edu; tpd10@psu.edu

Hruday Shah
Georgia Institute of Technology, Atlanta, GA 30332
e-mail: hshah316@gatech.edu

Janko Slavic et al. (eds.), *Computer Vision & Laser Vibrometry, Vol. 6*, Conference Proceedings
of the Society for Experimental Mechanics Series, https://doi.org/10.13052/97887-438-0151-1_17

order singular values of a decomposition [15]. Two methods, in particular, have been recently introduced for the direct de-noising of camera data for a modal decomposition [16, 17]. The first, presented at IMAC 2022 by Trainotti et al., uses the spatial density of the information to remove incoherent noise by use of low-rank reconstructions from the singular value decomposition (SVD) [16, 18]. In this work, the data is arranged in three different orientations leading to PRANK: a standard "FRF" orientation with drive points by accelerometers by frequency; a "flattened response" or "principle response function" orientation (PR-), where the data is rearranged to be frequency by all motion; and a "Hankel" form, where each drive-accelerometer response is rearranged into a Hankel matrix (-ANK). The SVD on each of these matrices produces a different effective filtering, helping to force outliers into higher singular values while maintaining prominent features. The second comes from the fluids community, where Scherl et al. leveraged Robust Principle Component Analysis (RPCA) [19] towards the modal decomposition in corrupted and noisy measurements of fluid flows. Here, RPCA aims to separate the raw image frames into a low-rank representation and a sparse matrix of outliers, much in the same aim as PRANK. Perhaps the most attractive aspect of RPCA is the rigorously defined minimization problem that underlies the regularization—the"robust" portion of RPCA—through which the rank to maintain is found with no user input. Given the proof of concept for RPCA was done on particle image velocimetry, the results should prove analogous for structural vibration measurements with digital image correlation and optical flow.

The final approach mentioned here shows high promise by use of regularization and known, trusted sparse measurements [20–22]. In these works, noisy high-speed camera data is combined with a sparse set of high-fidelity sensor data to resolve motion originally below the noise floor. In the initial approach by Javh et al. [20], an accelerometer is used to identify eigenvalues while the full-field camera data is used to identify mode shapes/modal constants. When used together in a Least-Squares Complex Frequency or Least-Squares Frequency-Domain method approach, the combined information was used to reconstruct the frequency response functions, showing modes originally below the noise floor of the camera. However, while resonances were captured, the neighboring regions in the real and imaginary parts experienced some issue. This work was improved soon after in [21, 22], which followed a similar motivation. In addition to merging data from parallel modal processes, a substructuring approach known as system equivalent model mixing (SEMM) is used. Typically, SEMM involves a model and a sparse data set from the structure; these are combined to update the dynamics of the model. Here, the full-field camera data is used as the parent model, and the sparse measurements come from more traditional, high fidelity sensors like laser doppler vibrometers and accelerometers. This technique showed improvements to [20], correcting the apparent phase issues.

These works provide tractable avenues for camera denoising, and merit use and observation on typical displacement measurements. The paper proceeds by motivating the theory briefly for each of these techniques. Next, we move to comparing their performance—from a user's perspective—on both temporal and spatial denoising efficacy for synthetic and experimental data. Further work and conclusions follow towards camera-based modal force reconstruction.

Background

The three methods investigated are outlined herein: PRANK [16], RPCA [17], and SEMM [22].

PRANK [16] can be thought of as an extension to the well practiced idea that noise is represented by the higher singular values of a decomposition, meaning a low-rank representation can be reconstructed which removes noise and improves quality. As discussed in the introduction, PRANK leverages continuity and smoothness across multiple data orientations. Within the PRF orientation, the data are represented as input-output FRFs across frequency, where the low rank representation can be related to the surface averaged receptance. If there exists an apparent resonance in a single input-output FRF, this would be removed in a low-rank representation. Likewise, spuriosities caused by typical camera-based displacement errors (e.g., super-pixel motion for optical flow), would also be evident in this representation, as the clipping of the displacement conveys broadband features not present across all FRFs. The Hankel orientation overlaps sections of an individual input-output FRF, where the low-rank representation acts as a moving average. This behaviour is due to the high-ranking of random measurement noise over increasing frequency; in addition, the low-rank representation may not provide a hankel matrix, and so enforcing this form by a diagonal average of assumed-equal quantities provides additional denoising. These two orientations can be done in series or parallel to varying effect, as described by the authors. PRANK can be understood pictorially in Figure 1.

RPCA [17] again can be understood to be a regularized implementation of the SVD, where the impacts of outliers in the regression is minimized. Specifically, RPCA aims to separate principal components, $\mathbf{L}$, from a sparse matrix of outliers, $\mathbf{S}$ that together form the input $\mathbf{X}$. This specific implementation described is a probabilistic proxy for the intractable optimization

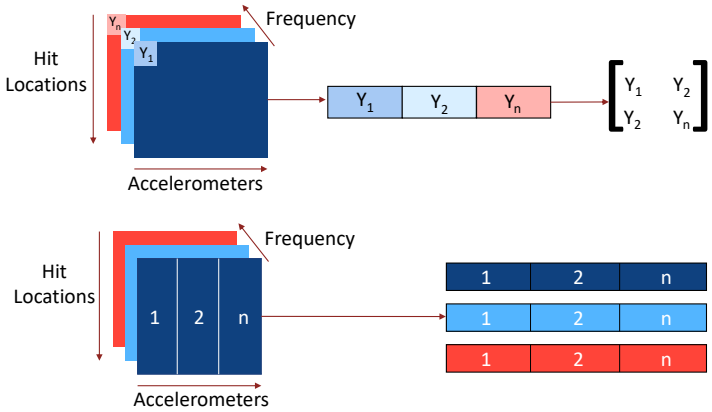

Fig. 1 PRANK Orientations: Hankel (top) and PRF (bottom).

problem, resulting in the form

$$\min_{\mathbf{L},\mathbf{S}} \|\mathbf{L}\|_* + \lambda_0 \|\mathbf{S}\| \text{ subject to } \mathbf{L} + \mathbf{S} = \mathbf{X} \tag{1}$$

where $\|\cdot\|_*$ represents the nuclear norm, and λ_0 is the hyper parameter given by $\lambda_0 = \lambda/\sqrt{max(n,m)}$ for an input matrix $\mathbf{X}$ of size $m \times n$. The proxy converges to the true optimization problem if $\lambda = 1$, given that $\mathbf{L}$ is not sparse and $\mathbf{S}$ is not low rank. Scherl et al. found these assumptions may only be partially valid for PIV data, such that λ may need to be varied slightly, in practice.

SEMM [22] aims to regularize the noisy camera data by the introduction of a number of trusted, high signal-to-noise measurements (e.g., accelerometers) at coincident degrees of freedom (DoF). The technique, pulled from dynamic substructuring, attempts to enforce compatibility at such shared DoF between a parent (camera data) and overlay model (accelerometer). Here, this is done using the reconstructed FRFs, found using the combined camera/accelerometer method from Javh et al. [20] and the polyreference least-squares complex frequency-domain method [23].These reconstructions serve as the parent model and the same accelerometer FRFs as the overlay. The aim, then, is the accelerometer will provide final corrections to the reconstructed camera FRFs as it would if the parent model were a finite element solution. The final calculation for a hybrid SEMM model is performed using the Lagrange Multiplier Frequency-Based Substructuring (LM FBS) single line formulation

$$\mathbf{Y}^{SEMM} = \mathbf{Y}_{gg} - \mathbf{Y}^{par}_{gg}(\mathbf{Y}^{rem}_{bg})^{+}(\mathbf{Y}^{rem}_{bb} - \mathbf{Y}^{ov}_{bb})(\mathbf{Y}^{rem}_{gb})^{+}\mathbf{Y}^{par}_{gg} \tag{2}$$

where $\mathbf{Y}^{par}$ is the parent model (camera mobilities), $\mathbf{Y}^{ov}$ is the overlay model (sensor mobilities), $\mathbf{Y}^{rem}$ the removed DoF from the parent model, and $\mathbf{Y}^{SEMM}$ the final hybrid model.

Analytical Plate

It was of interest to replicate a typical measurement scenario on a structure more complex than a one-dimensional beam or mulitiple degree-of-freedom oscillator. The main model used was a forced thin rectangular plate, whose equation of motion goes as

$$D\nabla^4 w(x,y,t) + \rho h \frac{\partial^2 w(x,y,t)}{\partial t^2} = F(x,y,t) \tag{3}$$

for D, w, ρ, h, and F being the flexural rigidity, displacement, mass density, thickness, and forcing fuction, respectively. Simple supports were assumed so to model the plate analytically. Time harmonic, steady state solutions in the homogeneous case follow as

$$w(x,y,t) = \Phi(x,y)T(t) = \sum_{m,n} A_{mn} \sin\frac{m\pi x}{L_x} \sin\frac{n\pi y}{L_y} e^{j\omega_{mn}t} \tag{4}$$

for some mode number m, n, with modal participation $A_{m,n}$ and natural frequency ω_{mn} given by

$$\omega_{mn} = \sqrt{\frac{D}{\rho h}}\left[\left(\frac{m\pi}{L_x}\right)^2 + \left(\frac{n\pi}{L_y}\right)^2\right].$$

This plate was driven over twenty unique points, whose response was composed of the first 175 modes. Panel area discretization was 33×35, allowing for a sufficient number of points per wavelength up to the modes of interest. Artificial damping and noise were applied, and the plate was allowed to decay over the record. These displacements were then converted to mobility for use in the methods. For reference, this matrix is 1155 outputs $\times$ 20 inputs $\times$ 2000 frequency bins.

Looking first at the results from PRANK, Figure 2 illustrates extremely good visual agreement between the analytical model input and PRANK output over multiple DoF. While only a subset is shown, the effect over the surface may be summarized using the surface averaged mobility given in Figure 3. Again, PRANK is seen to reveal all of the underlying dynamics of the structure, including those which are highly damped and an order of magnitude below the modeled camera noise floor. The frequency response assurance criterion ($FRAC$) is used to assess the degree of similarity between the surface averages. For PRANK, the $FRAC$ is found to be $FRAC = 0.9979$, indicating high similarity between the two as in the visual comparison.

Moving now to the RPCA results, Figure 4 shows the denoised mobilities using a $\lambda = 0.33$—a value found to work well on other camera datasets, and in agreement with Scherl et al.'s need to reduce λ for realistic data. It is clear that this value made for too aggressive of a filter, reducing magnitudes by more than half. That said, dynamics of similar contour are revealed below the noise floor. Figure 5 shows this effect more clearly. Given the reduction of the noise floor, the surface average is now much closer in contour to the model input albeit lower than the true magnitude. Here, the $FRAC$ calculation gives $FRAC = 0.6021$, likely due to the similar curvature but varied magnitudes. Clearly the results suggest an increase in the hyper parameter to reduce the aggressive filtering and improve agreement.

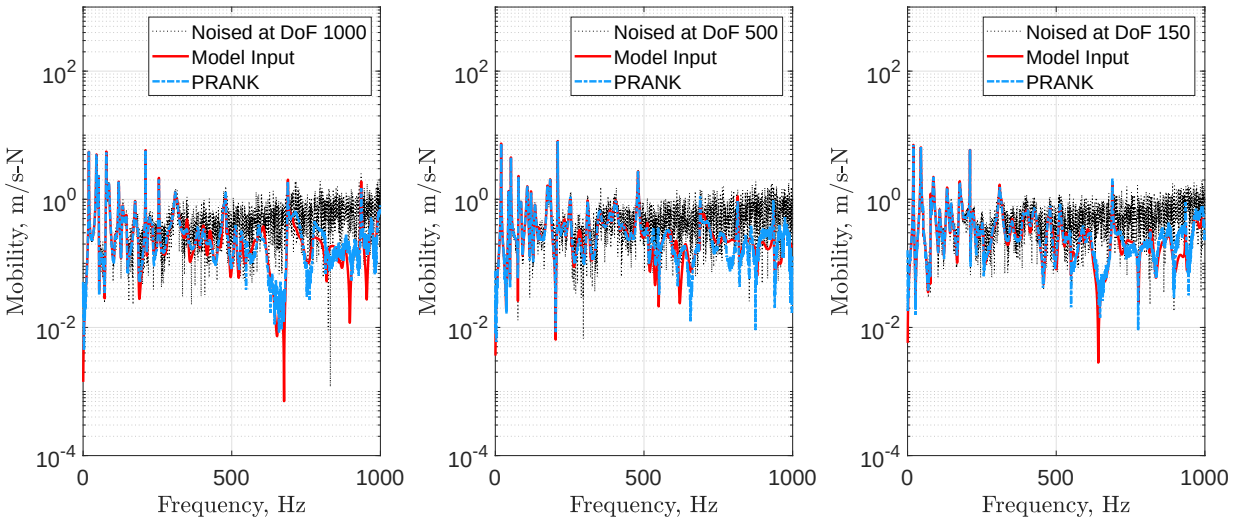

Fig. 2 Random mobilities compared between noised (model output), model input, and PRANK output.

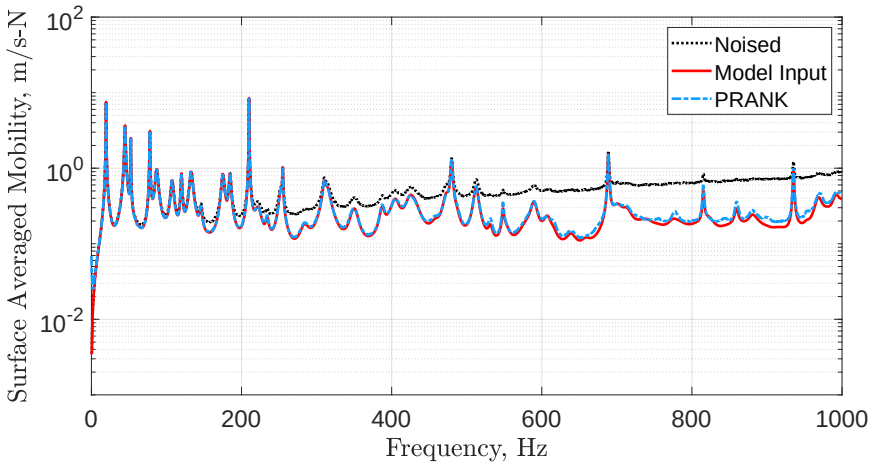

Fig. 3 Surface averaged mobilities compared between noised (model output), model input, and PRANK output.

Hence, we now consider RPCA using a $\lambda = 1$, to both reduce the impact of the filter as well as investigate the ideal case. Figure 6 shows the improvement of the data reduction using the higher λ value. Now, the performance of RPCA is comparable to PRANK, though it is observed that the relative magnitudes are still affected and there remains a considerable amount of noise at higher frequencies. The surface averaged mobility of Figure 7 again shows improvement using the higher value, now falling well on the model. Here, the $FRAC$ value gives $FRAC = 0.9780$—still below that of PRANK, but much improved over the more aggressive filtering. However, RPCA on datasets of this size is computationally quite expensive, with this data reduction being on the order of 6-12 hours (1000 to 2000 iterations), compared to the few minutes needed for PRANK. Given the regression is dependent on the number of observations, it is not tractable to run a subset to estimate the ideal λ. Indeed, the authors were able to rerun the estimate, but such a repeat is non-ideal. These results imply utility, but also impracticality of RPCA for large camera-based datasets when compared to PRANK.

Finally, we consider the camera-accelerometer hybrid reconstructions and subsequent corrections done using SEMM.

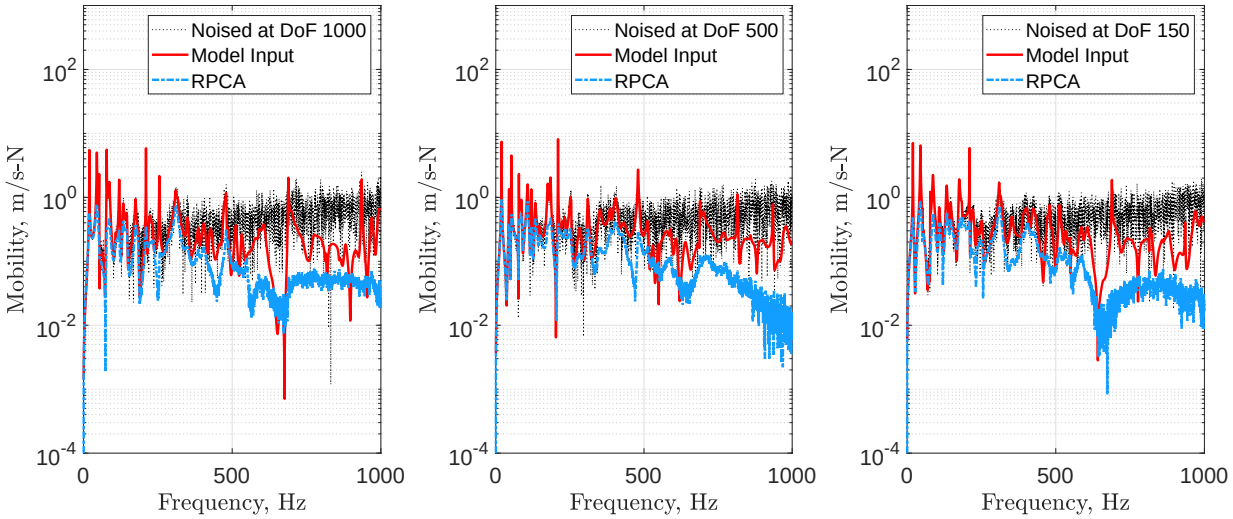

Fig. 4 Random mobilities compared between noised (model output), model input, and RPCA output ($\lambda = 0.33$).

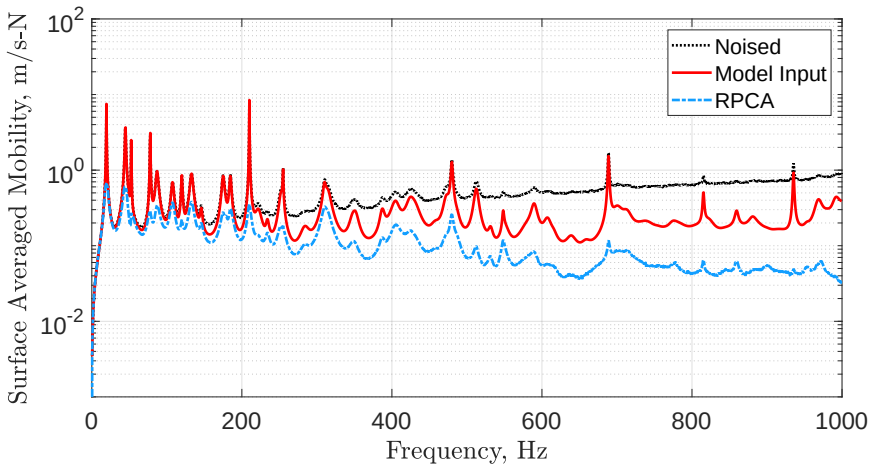

Fig. 5 Surface averaged mobilities compared between noised (model output), model input, and RPCA output ($\lambda = 0.33$).

Certainly, the technique is the most technically involved: a modal parameter estimation must be done using the overlay, reference signals; mode shapes must then be calculated from the estimated modal parameters and noisy camera data; reconstructions of the FRFs are then created; finally allowing for their use in SEMM to refine the reconstructions. With this all being so, these techniques are seen to visually perform the best compared to PRANK and RPCA. As before, the random mobilities are presented in Figures 8, 10 and surface averaged mobility in Figures 9, 11. While the surface average between PRANK, the hyrbid reconstruction, and SEMM are visually quite close, the subtle out-perfomance in estimating the zeros, in parallel to the tighter fit of damping and magnitude show these last techniques to be the most robust, if being the most user involved.

Considering first the hyrbid method alone, the $FRAC$ between the hybrid results and model input gives $FRAC = 0.9995$, indicating almost perfect agreement, and a quantitatively better reconstruction than PRANK.

Interestingly, the $FRAC$ between SEMM and the model input is slightly lower, with $FRAC = 0.9968$. This slight reduction in performance can be seen visually in both the random mobilities and the surface average. Further, it is clear

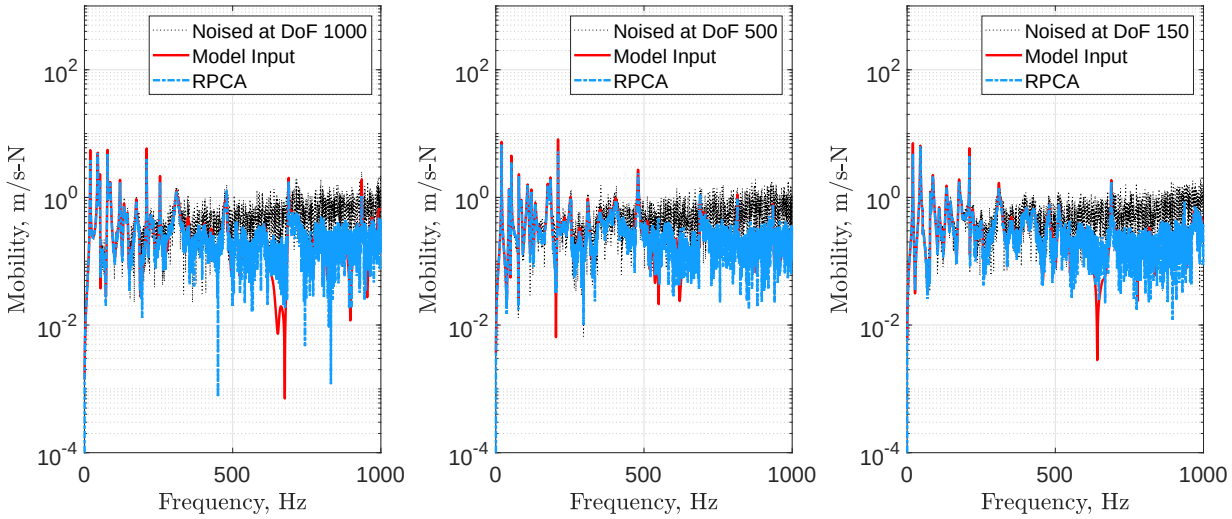

Fig. 6 Random mobilities compared between noised (model output), model input, and RPCA output ($\lambda = 1$).

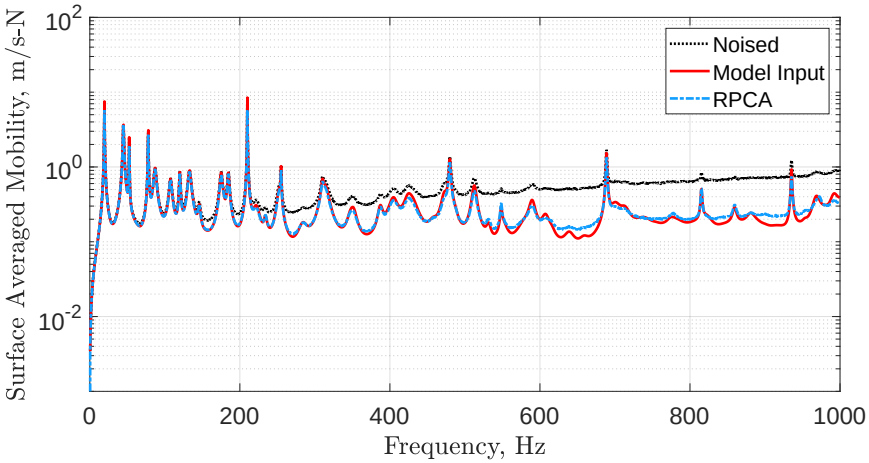

Fig. 7 Surface averaged mobilities compared between noised (model output), model input, and RPCA output ($\lambda = 1$).

that much of refinement of SEMM has been in amplitude, and not adjustment of the dynamics approximated by the FRF reconstructions. It is possible that the performance was biased by the accelerometer locations chosen, and this thought is supported by the varied performance in the random mobilitie. If the overlay accelerometers chosen happen to have all missed a portion of dynamics, the over-compensation in the sub-structuring stage would follow logically. In future work, such possible sensitivity to the performance of SEMM will be explored.

Experimental Beam

For the experimental dataset, a 0.43 m aluminum cantilever beam ($E = 68\,\text{GPa}$) was struck with an instrumented modal hammer, as seen in Figure 12. A Phantom v1212 high-speed camera was used to record video data at a resolution of 800×1280 and rate of 5000 frames per second. Constant lighting was used to preserve brightness constancy and a black

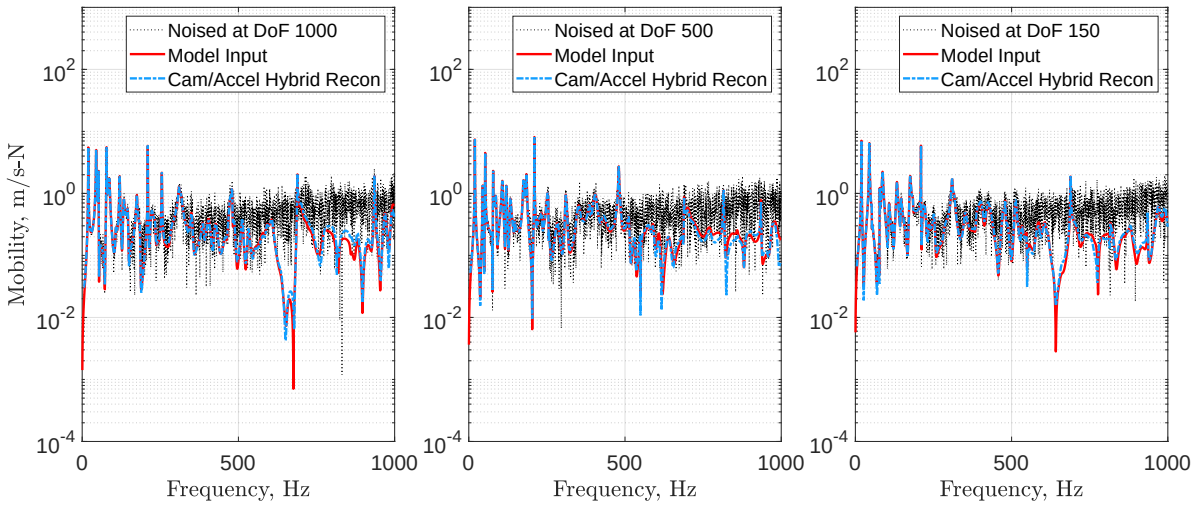

Fig. 8 Random mobilities compared between noised (model output), model input, and hybrid output.

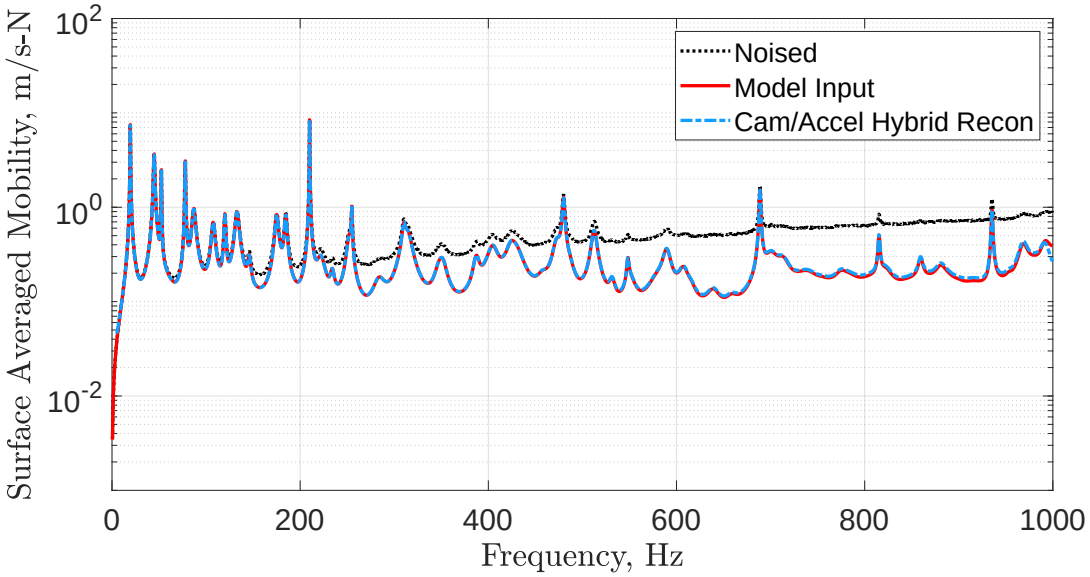

Fig. 9 Surface averaged mobilities compared between noised (model output), model input, and hybrid output.

background was used to promote good contrast at the edge for motion extraction. Camera and setup parameters led to a calibration factor of 0.4658 $\frac{mm}{px}$. Further details of the setup can be found in [1].

A laser doppler vibrometer (LDV) aimed near the tip of the beam serves here as the reference and overlay model. As before, each method was applied to the matrix of mobilities from a SIMO test of the beam. For reference, this matrix is 905 outputs $\times$ 1 input $\times$ 2000. It is worth noting that this implies substantially fewer observations for the data reduction techniques than in the analytical case. Further, we do not consider SEMM here, as the single reference is not expected to improve results of the camera-accelerometer hybrid.

Figure 13 presents the results of the three techniques on the beam SIMO data. It is evident that the effect is lost here, with both PRANK and RPCA failing to reveal much if any of the underlying dynamics beflow the camera noise floor. Indeed, where PRANK was almost identical in result to SEMM in the analytical case, the overall lack of observations is shown to be a detriment to the method. This follows intuitively, and should be of no surprise. Further while RPCA is seen to fail at

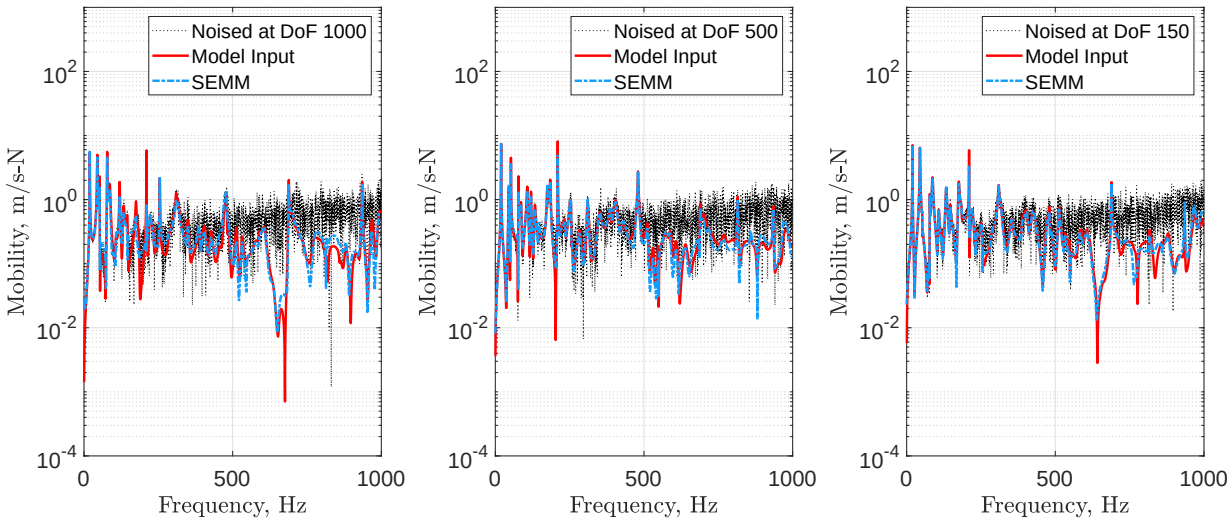

Fig. 10 Random mobilities compared between noised (model output), model input, and SEMM output.

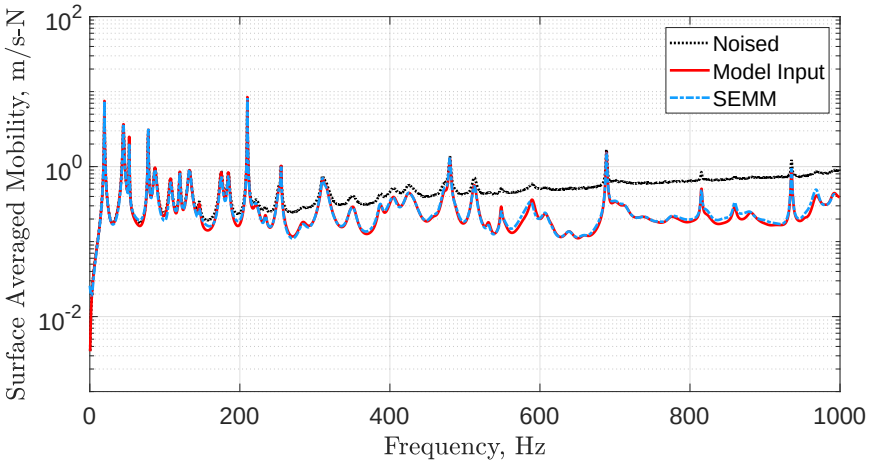

Fig. 11 Surface averaged mobilities compared between noised (model output), model input, and SEMM output.

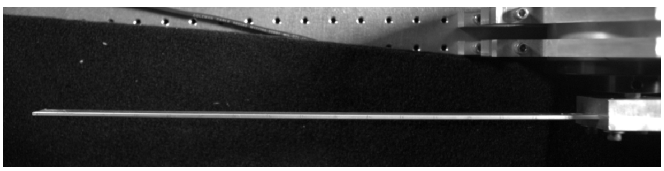

Fig. 12 Video frame of cantilevered beam, showing sharp contrast

identifying any new dynamics, it does reduce the camera noise floor by an order of magnitude, which may be beneficial for time-domain analysis of lower-frequency behavior, such as below 500 Hz. When considering SEMM, the initial, visual results appear quite good: the noise has been removed and pole-zero behaviour is now apparent. Both of these factors are important for accurate and stable camera-based modal force reconstruction.

Turning to Figure 14, similar trends may be observed, where RPCA and SEMM appear to agree decently well to each other and the raw data below 500 Hz, with PRANK providing the least denoising. Overall, RPCA and PRANK have lowered the noise floor, but reveal no dynamics that are not already apparent in the raw surface average. What is also clear by comparing these techniques is the lack of magnitude retention between the raw data and any of the methods—particularly at the first resonance. While these curves may be visually appealing, and possibly sufficient to render higher-quality mode shapes, the modification of true magnitude will directly hinder the force reconstruction process. Indeed, such error in modal

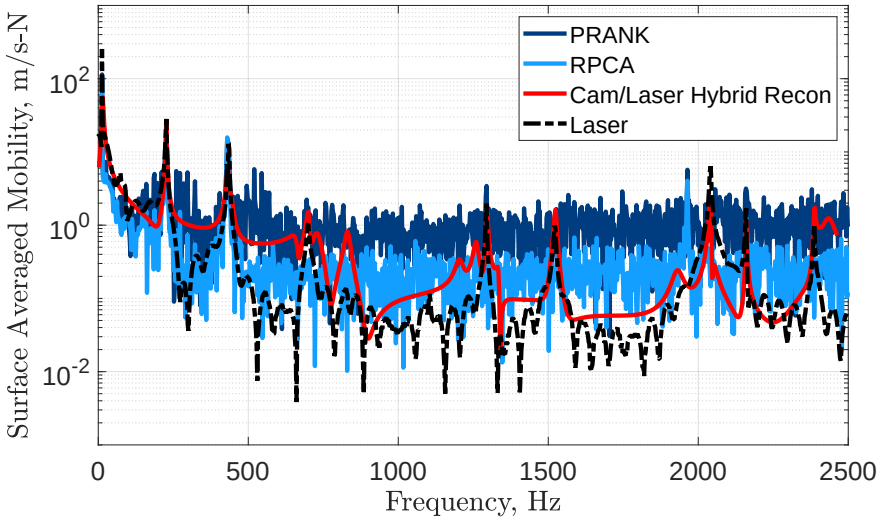

Fig. 13 Mobility comparison between the reference laser and denoising techniques, showing superior performance from the camera-accelerometer hybrid.

participation caused by noisy data is the exact problem the authors are attempting to solve.

Conclusion

Herein, we have aimed to evaluate and compare three recently introduced camera denoising techniques, and their efficacy for noise reduction towards a modal force reconstruction approach. Application to MIMO data showed great utility across all three methods, revealing underlying dynamics (e.g., modes, pole-zero behaviour) which were otherwise obscured by the camera noise floor. What was most encouraging was the ability of PRANK to reveal almost identical dynamics to the more-involved SEMM, both being in excellent agreement to the pure, analytical model input. When moving to SIMO data, the data reduction techniques were shown to struggle due to the overall lack of observations with good signal-to-noise. SEMM appeared again the most successful, though not without fault in terms of absolute magnitude. General conclusions from the users' perspective may be summarized as follows: PRANK and SEMM are comparable in cases with an abundance of inputs,

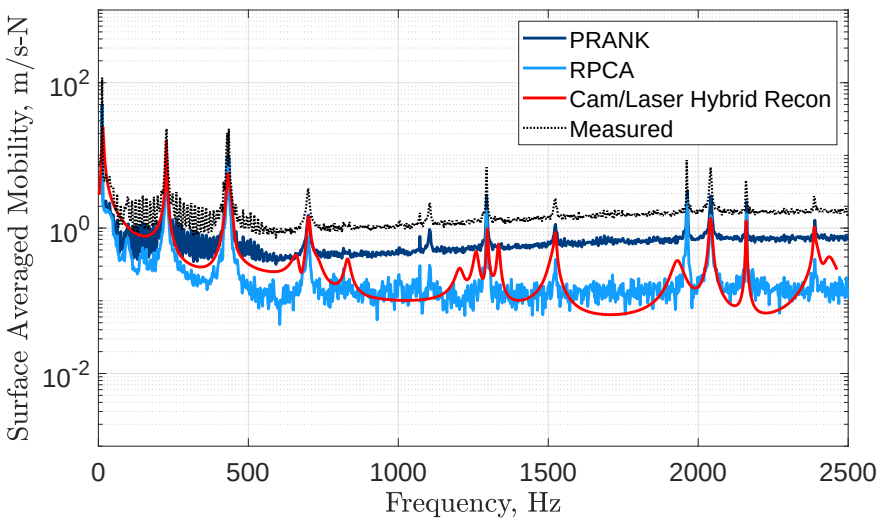

Fig. 14 Surface averaged mobility comparison between the reference laser and denoising techniques, showing superior performance from the camera-accelerometer hybrid.

outputs, and frequency bins, while RPCA appears to perform slightly worse and is computationally more expensive; Data reduction techniques such as PRANK and RPCA will inherently struggle when there are few datums of quality; and SEMM appears the most robust and trustworthy given the incorporation of a physics-informed regularization. As work progresses on modal force reconstruction—an inherently SIMO related process—the authors hope and are excited to see improvements to these techniques and their eventual application to worthwhile engineering problems.

Acknowledgments This work was partially supported by the PIPELINE: Penn State Intern PipelinE LInks to Navy Engineering program, ONR grant #N000142312656. The Penn State PIPELINE Program motivates and connects students and faculty to careers and research opportunities with the Navy technical workforce. The authors would also like to thank the ARL Walker Assistantship program, which provided support for acquiring the data used here.

References

1. Collier, S. and Dare, T. "Accuracy of phase-based optical flow for vibration extraction". *J. Sound Vib.* (2022)
2. Collier, S. and Dare, T. "Informed pixel pushing: A new method of large-motion handling for phase-based optical flow". *Measurement* (2023)
3. Collier, S. and Dare, T. "Regime sorting for multiscale vibration and phase-based motion extraction". In Di Maio, D. and Baqersad, J., editors, *Rotat. Mach., Opt. Methods & Scanning LDV Methods, Volume 6*, Cham (2023) Springer Int. Publ.
4. Baqersad, J., Poozesh, P., Niezrecki, C., and Avitabile, P. "Photogrammetry and optical methods in structural dynamics – a review". *Mech. Syst. Signal Process.*, 86:17–34 (2017)
5. Poozesh, P., Sarrafi, A., Mao, Z., Avitabile, P., and Niezrecki, C. "Feasibility of extracting operating shapes using phase-based motion magnification technique and stereo-photogrammetry". *J. Sound Vib.*, 407:350–366 (2017)
6. Rohe, D. and Reu, P. "Experimental modal analysis using phase quantities from phase-based motion processing and motion magnification". *Exp. Tech.*, 45:297–312 (2021)
7. Chen, J.G., Wadhwa, N., Cha, Y.J., Durand, F., Freeman, W.T., and Buyukozturk, O. "Modal identification of simple structures with high-speed video using motion magnification". *J. Sound Vib.*, 345:58–71 (2015)
8. Diamond, D., Heyns, P., and Oberholster, A. "Accuracy evaluation of sub-pixel structural vibration measurements through optical flow analysis of a video sequence". *Measurement*, 95:166–172 (2017)
9. Javh, J., Slavič, J., and Boltežara, M. "The subpixel resolution of optical-flow-based modal analysis". *Mech. Syst. Signal Process.*, 88:89–99 (2017)
10. Barron, J.L., Fleet, D.J., and Beauchemin, S.S. "Performance of optical flow techniques". *Int. J. Comput. Vis.*, 12:43–77 (1994)
11. Hay, J. "High dynamic range imaging for the detection of motion". *PhD Thesis,*, University of Louisville (Unpublished results)
12. Fleet, D.J. and Jepson, A.D. "Computation of component image velocity from local phase information". *Int. J. Comput. Vis.*, 5:77–104 (1990)
13. Wadhwa, N., Rubinstein, M., Durand, F., and Freeman, W.T. "Phase-based video motion processing". *ACM Trans. Graph.*, 32(4) (2013)
14. Lucas, B.D. and Kanade, T. "An iterative image registration technique with an application to stereo vision". In *Proc. 7th Int. Jt. Conf. Artif. Intell. - Volume 2*, IJCAI'81, page 674–679, San Francisco, CA, USA (1981) Morgan Kaufmann Publ. Inc.
15. Epps, B. and Krivitzky, E. "Singular value decomposition of noisy data: noise filtering". *Exp. Fluids*, 60 (2019)
16. Trainotti, F., Klaassen, S.B., Bregar, T., and Rixen, D.J. "A singular value based filtering strategy for noise reduction on measured response data". In *41th Int. Mod. Anal. Conf.*, pages 1–4. Unpublished (2022)
17. Scherl, I., Strom, B., Shang, J.K., Williams, O., Polagye, B.L., and Brunton, S.L. "Robust principal component analysis for modal decomposition of corrupt fluid flows". *Phys. Rev. Fluids*, 5:054401 (2020)
18. Trainotti, F., Slimak, T., and Rixen, D. "Towards full-field frequency based substructuring: an application case" (2024)
19. Candès, E.J., Li, X., Ma, Y., and Wright, J. "Robust principal component analysis?". *J. ACM*, 58(3) (2011)
20. Javh, J., Slavič, J., and Boltežar, M. "High frequency modal identification on noisy high-speed camera data". *Mechanical Systems and Signal Processing*, 98:344–351 (2018)
21. Bregar, T., Zaletelj, K., Čepon, G., Slavič, J., and Boltežar, M. "Improved frf estimation from noisy high-speed camera data using semm". In Di Maio, D. and Baqersad, J., editors, *Rotat. Mach., Opt. Methods & Scanning LDV Methods, Volume 6*, Cham (2020) Springer Int. Publ.
22. Bregar, T., Zaletelj, K., Čepon, G., Slavič, J., and Boltežar, M. "Full-field frf estimation from noisy high-speed-camera data using a dynamic substructuring approach". *Mechanical Systems and Signal Processing*, 150:107263 (2021)
23. Peeters, B., Van der Auweraer, H., Guillaume, P., and Leuridan, J. "The polymax frequency-domain method: A new standard for modal parameter estimation?". *Shock and Vibration*, 11(3-4):523692 (2004)